Modelling of Crack Growth Based Acoustic Emission Release in Aluminum Alloys

Markus G. R. SAUSE *
*University of Augsburg, Augsburg, Germany

Abstract. Various theories in the past have addressed the correlation of material properties and the respective acoustic emission release during fracture. Whilst these theories yield good predictions for fundamental relationships, they neglect the dynamic displacements during crack formation. This paper presents first results for a new acoustic emission crack source model based on a finite element modelling approach which calculates the dynamic displacement field during crack formation. The specimen modelled is statically loaded until conditions for crack growth (e.g. local exceedance of material's fracture toughness) are fulfilled. Crack growth is modelled by local degradation of the material properties in the crack process zone. The respective displacements generate the acoustic emission signal and allow detailed examination of the generation of acoustic emission signals. Subsequent to crack growth signal propagation in a simple tensile specimen is modeled. The signal propagation is modeled superimposed to the static displacement field. The influence of the crack propagation length, the static displacement field and material plasticity is investigated. It is demonstrated, that present analytical theories systematically underestimate the strength of acoustic emission sources. Strong discrepancy was found between the rise-times predicted by the present simulations and those assumed in analytical theories.

1. Introduction

The formation and propagation of cracks in solid media is a field of research that has been active for decades. Still, the theoretical description of the physics at the crack tip and the crack dynamics are active fields of research. A phenomenon that is closely related to the crack dynamics is the generation of acoustic waves due to the crack formation and motion. These acoustic waves propagate within the solid and can be detected at the surface by suitable sensor systems. Despite of the broad range of technical applications, only little work has been performed recently to advance the understanding of the physical processes involved in the generation of such acoustic emission signals.

In order to interpret the detected acoustic emission signals in terms of their relevance to material failure it is required to have concise knowledge of the underlying physics. The whole process can be categorized into three subsequent parts. The first part comprises the acoustic emission source, the second part considers the acoustic emission signal propagation from source to sensor and the third part consists of the acoustic emission signal detection.

In the past, various valuable attempts have been made to provide a theoretical description of acoustic emission sources. The source model concept used in most of the

analytical approaches was derived from seismology and is based on the early work of K. Aki and P. Richards [1]. Here, source models are geometrically approximated as point sources, while the dynamic of the source are either approximated from iterative refinement of model parameters to fit experimental data or are based on assumptions. Various step-function descriptions exist, which are used to describe the 3-dimensional spatial displacement of the crack surface during crack formation [2-5]. In particular the rise-time of the initial crack surface displacement is an essential parameter to describe the crack surface motion [6]. However, it is difficult to measure the rise-times of crack propagation experimentally. Therefore, the rise-time is typically estimated based solely on the elastic properties of the bulk material. Despite of this drawback, this type of source modeling has been successfully applied to many cases and the basic concept has been used within the generalized theory of acoustic emission by Ono and Ohtsu [3,7], the work of Scruby and Wadley [8] and numerous other analytical descriptions [2,4,9].

In recent years it has become more convenient to use numerical methods to model acoustic emission sources. In this field, Prosser, Hamstad and Gary applied finite element modeling to simulate AE sources based on body forces acting as point source in a solid [5,10]. Hora and Cervena investigated the difference between nodal sources, line sources and cylindrical sources to build geometrically more representative acoustic emission sources [11]. At the same time, we proposed a finite element approach using an acoustic emission source model taking into account the geometry of a crack and the inhomogeneous elastic properties in the vicinity of the acoustic emission source [12]. Currently all these source models require an explicit source function. Therefore, no details of the dynamics arising from the crack formation process and the subsequent crack surface motion are taken into account.

In contrast to the source model, the theoretical description and numerical implementation of wave propagation is already well established [5,9,10,12,13]. However, it is important to consider the effects of attenuation, dispersion and propagation in guiding media to accurately capture the characteristics of the signal (e.g. frequency content). While analytical descriptions benefit from the low computational intensity [9] to describe wave propagation, for the numerical methods a main focus is the improvement of the calculation routines.

Another challenge to obtain acoustic emission signals to compare to experimental data stems from the description of the detection process. Here the detection process using piezoelectric sensors can have significant impact on the bandwidth of the detected signals and their relative frequency content. While some analytical approaches consider the sensors transfer function explicitly [9,14] some attempts have also been made to model the response of piezoelectric sensors themselves [15]. Recently a finite element approach to directly include the piezoelectric sensor in a modeling environment to also account for the interaction between the sensor and the material it is mounted on was proposed [16].

In the present work, a mode-I crack in an aluminum alloy is modeled as acoustic emission source. The aim of the investigation is the comparison between predictions of analytical theories and the new source model description. Fundamental material properties are varied and their impact on the obtained acoustic emission signals is discussed.

2. Simulation method

The type of finite element modeling used is based on the calculation of stress-strain relationships in a specimen volume governed by the structural mechanics constitutive equation. Based on the principle of virtual work the finite element program COMSOL

solves the partial differential equations for equilibrium conditions, expressed in global or local stress and strain components.

The geometry chosen for the present investigation is shown in figure 1. The tensile specimen is modeled as simple bar with edge length of 100 mm × 40 mm (height × width) and 2 mm thickness. For simplicity all calculations are carried out in a 2D cross-section using plain strain conditions. The through crack occurs at the center of the specimen and affects the full thickness as seen in the inset in figure 1. The length of crack growth a is chosen as free parameter in the following. For reasons of symmetry at the yz-plane, the 2D plane calculated can further be reduced to one half of the full cross-section (marked in red).

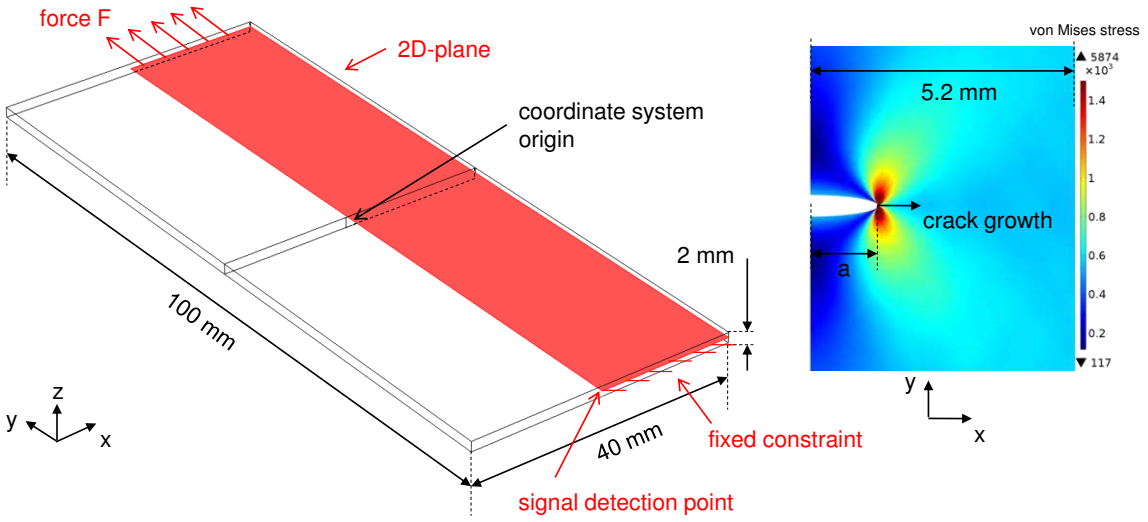

Fig. 1. Tensile specimen geometry used in the simulations. Red plane marks 2D-part modeled using plain strain conditions. Deformation of crack surface exaggerated by 10-times to allow visual representation of crack position with superimposed von Mises stress for an external force of 25 kN.

In the present simulation Hook's law is chosen as constitutive equation. For the case of aluminum alloy used herein, the linear elastic behavior is described using the Young's modulus E, Poisson's ratio ν and density ρ given in table 1. For modeling of elasto-plastic behavior a strain-hardening approach using a superposition of two exponential functions with yield strength σ_y as given in table 1 is applied. The total stress σ_{ys} after yielding is calculated as:

$$\sigma_{ys} = \sigma_y + \sigma_h(\varepsilon_p)$$

In the first step, the static displacement field is calculated as function of an external tensile force F applied in the y-direction. The edge opposite to the applied force is kept at a fixed position as boundary constraint. Subsequently, the occurrence of crack propagation along the x-direction is modeled using a thin elastic layer defined at the edge coincident with the x-axis. The stiffness k of the thin elastic layer is chosen as follows:

$$k = \begin{cases} k_0 \; if \; undamaged \\ 0 \; if \; damaged \end{cases}$$

The initial stiffness is derived from the elastic properties of the material to be $k_{0,n} = 1.0 \cdot 10^{20}$ [N/m³] and $k_{0,t} = 2.6 \cdot 10^{19}$ [N/m³] for the direction normal and transverse to the load axis, respectively. In principle, the degradation rule can be formulated as classical failure criterion. However, to investigate some basic relationships it was found numerically more stable to provide the damage state explicitly as function of time. Therefore, fully unstable crack propagation with a velocity identical to the maximum allowed Rayleigh

velocity is assumed in the following. Acceleration and deceleration at the beginning and at the end is assumed to be negligible.

Mesh resolution was chosen to be a maximum of 25 µm edge length along the crack plane with a gradual increase towards 500 µm on the global scale. Calculations were carried out using a time step of 1 ns for a total length of 10 µs. Sufficiency of these settings was proven following the method proposed in [13] using half the mesh resolution and time step as reference case.

Table 1. Material parameters of aluminum alloy used in the investigation.

Name	**value**	**Name**	**value**
Young's modulus Poisson's ratio Density Yield strength	69.9 [GPa] 0.33 2700 [kg/m³] 275.3 [MPa]	Strain hardening function	$\sigma_h(\varepsilon_p) = 147 \cdot 10^6 \cdot \left(1 - e^{-\frac{\varepsilon_p}{0.0933}}\right) + 77.8 \cdot 10^6 \cdot \left(1 - e^{-\frac{\varepsilon_p}{0.0088}}\right)$

3. Results and Discussion

3.1 Source Operation

Due to the presence of the static displacement field, the degradation of the elastic properties at the thin elastic layer causes an excitation of an acoustic wave as shown in a sequence of images in figure 2. Until t = 343 ns the crack grows with a total length of 1.0 mm. The near-field of the crack can be differentiated into two major contributions. One part stems from the crack opening and would be directed perpendicular to the crack surface. The second part originates from the advance of the crack tip and radiates slightly off-axis relative to the propagation direction. At the moment of crack arrest, the two contributions develop into two waves, referred to as "primary wave" and "secondary wave" in the following. Approximating this mode-I crack as single dipole would generate a contribution which is mostly due to the "primary wave". Improved representations like a model using three orthogonal dipoles are able to capture parts of the behavior of the "secondary wave" [8]. However, the quantitative relation of their contributions is dominated by the strength of the force extensions modeled for the three dipoles and not by the underlying crack dynamics.

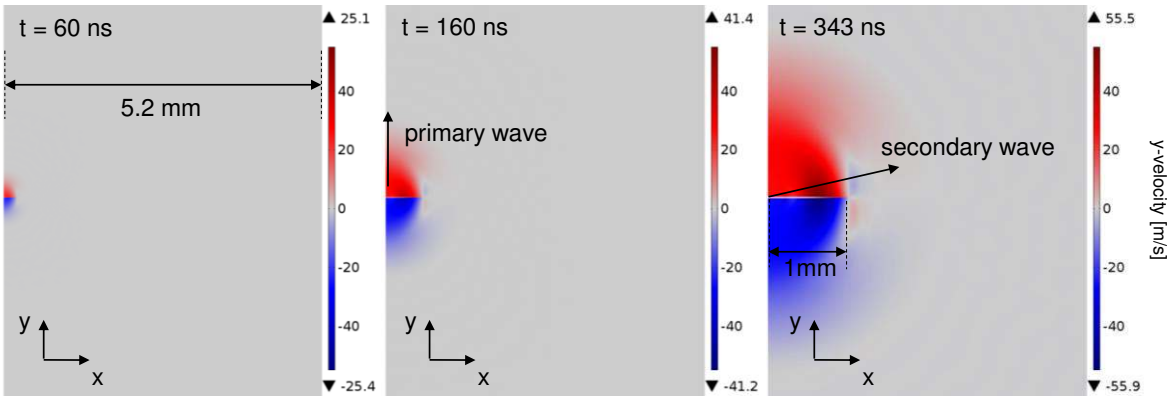

Fig. 2. Formation of the "primary wave" and "secondary wave" in the near-field of the crack shown in a sequence of times after crack initiation.

In the far-field these two waves propagate to the boundaries of the specimen and are reflected back into the volume (see figure 3). In the following, variations of the external loading and the crack progress are investigated. Therefore, the maximum y-displacement of

the free crack surface positioned initially at (x,y) = (0,0) mm is evaluated. Comparison is made to the observed y-displacement at a hypothetical sensor position at (x,y) = (0,50) mm.

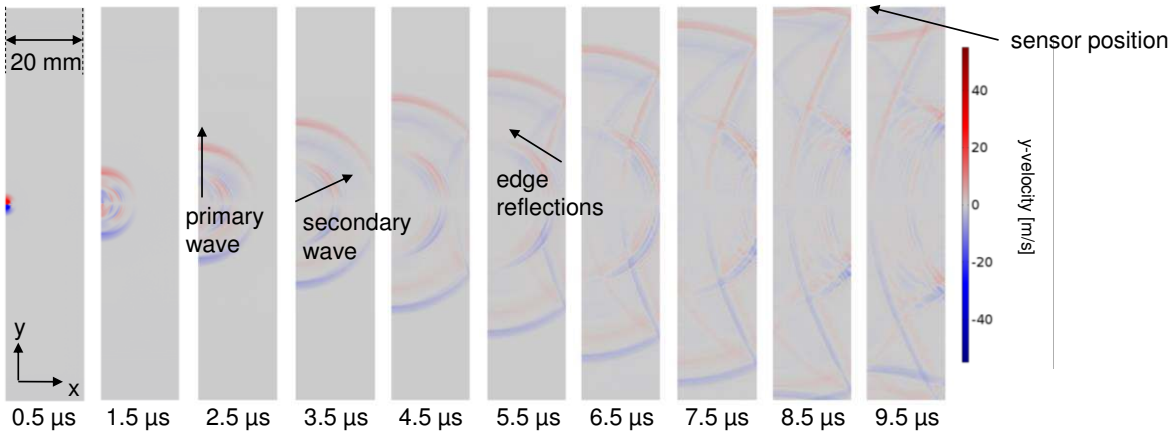

Fig. 3. Propagation of acoustic waves in the far-field of the crack for a sequence of times after crack initiation.

3.2 Influence of Crack Length

First a comparison is made between the results of three different crack propagation lengths. Therefore the length of the thin elastic layer is adjusted to allow crack propagation for 0.5 mm, 1.0 mm and 1.5 mm. The respective evaluation of the y-displacement of the crack surface is shown in figure 4-a. During the duration of crack propagation, the y-displacement increases linearly. However, at the moment of crack arrest, the y-displacement does not stop or cease, but increases further until a maximum value is reached. Subsequently, the crack surface starts to vibrate and settles at a new equilibrium position. The predictions of the y-displacement derived from the theory of Green [17] are marked as dashed lines in figure 4-a. As can be seen from the comparison, in the initial part these values are systematically lower than the present model predictions. This originates from the underlying assumptions in the theory. In [17] static crack opening is assumed, i.e. the length of the crack is already present as flaw in the material and merely opens due to an external force. If the same assumptions are made in the present model, the achieved deformation state is in 99% agreement to the values predicted by [17]. However, the dynamic crack propagation seems to generate initial acoustic emission amplitudes larger than predicted by those analytical theories.

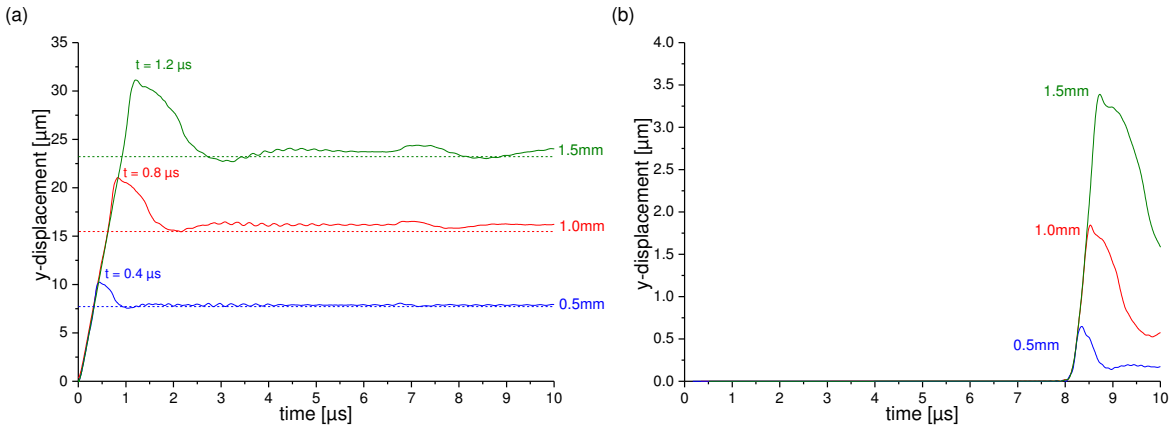

Fig. 4. Evaluation of source displacement (a) and surface displacement at (x,y) = (0,50) mm (b) as function of crack length.

At the sensor position, the first noticeable y-displacement occurs after signal propagation from the crack source to the sensor as seen in figure 4-b. This is due to the “primary wave” visible in figure 3. Subsequently, contributions from the “secondary wave” arrive and superimpose with the “primary wave”. For an increased length of crack propagation the individual contributions of the y-displacement increase accordingly.

3.3 Influence of Applied Load

Next, the external load used to generate the superimposed static displacement field is varied from 5 kN to 10 kN and 25 kN. This is to model the occurrence of cracks with varying accumulated energy at the position of the crack zone. As seen in figure 5-a the temporal behaviour of the calculated y-displacement of the crack surface is mostly identical to the previous investigation. Since the crack length was kept constant at 1 mm, the maximum occurs at the same time t = 0.8 µs. For comparison, the y-displacement predictions according to the theory in [17] are added as dashed horizontal lines. For the y-displacement obtained at the sensor position shown in figure 5-b an increasing amplitude for an increasing external load before fracture is observed.

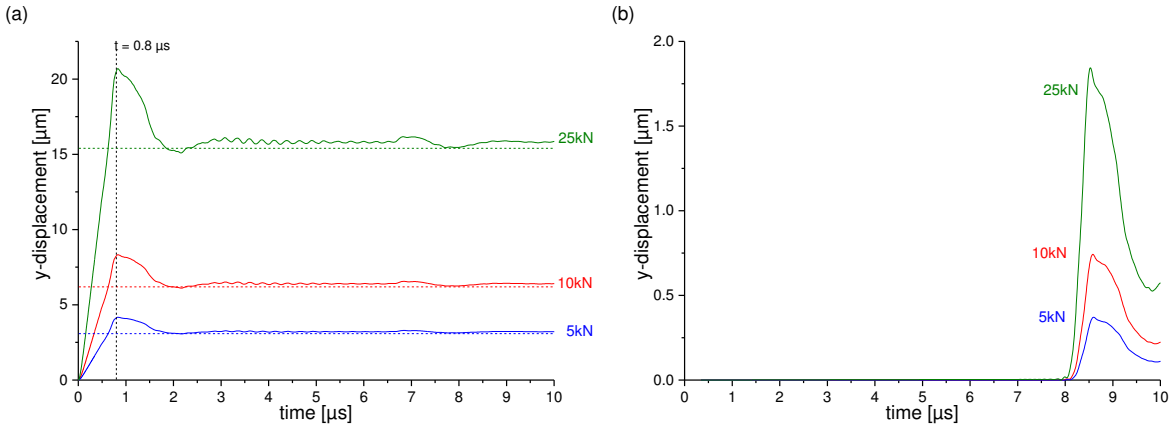

Fig. 5. Evaluation of source displacement (a) and surface displacement at (x,y) = (0,50) mm (b) as function of external load.

3.4 Influence of Plasticity

Since many materials show excessive plastic deformation before fracture, the impact of this deformation is subject to the next investigation. For the aluminum alloy used herein, we follow a strain-hardening approach as given in table 1. Figure 6-a and 6-b compare the calculation results using a linear elastic material model and the elasto-plastic description for the y-displacement of the crack surface and the y-displacement at the sensor position. In both cases an external force of 25 kN and a crack length of 1 mm was chosen. After crack initiation the additional plastic deformation causes a first settling of y-displacement at around 25 µm, which is at least two times larger than for the linear elastic case. Accordingly, the effective rise-time of the crack is substantially larger. Due to additional plastic deformation at the crack tip, a further increase of y-displacement occurs. No oscillation of the crack surface comparable to the linear elastic case is observed. For the acoustic emission signals detected at the sensor position, additional effects come into play. Since macroscopic yielding of the specimen superimposes the dynamic displacements, the overall signal is dominated by the increasing plastic deformation of the specimen. This first leads to a decrease in y-displacement, but then increases steadily far beyond the 10 µs shown in figure 6-b. However, a real sensor applied at this position would not be affected by the low frequency components in the signal. Filtering by a 50 kHz 10^{th} order Bessel

high-pass reveals the onset of the signal to be around 6.6 µs as seen from the inset in figure 6. This preliminary onset is caused by the hardening of the specimen, which causes an increase in sound velocity.

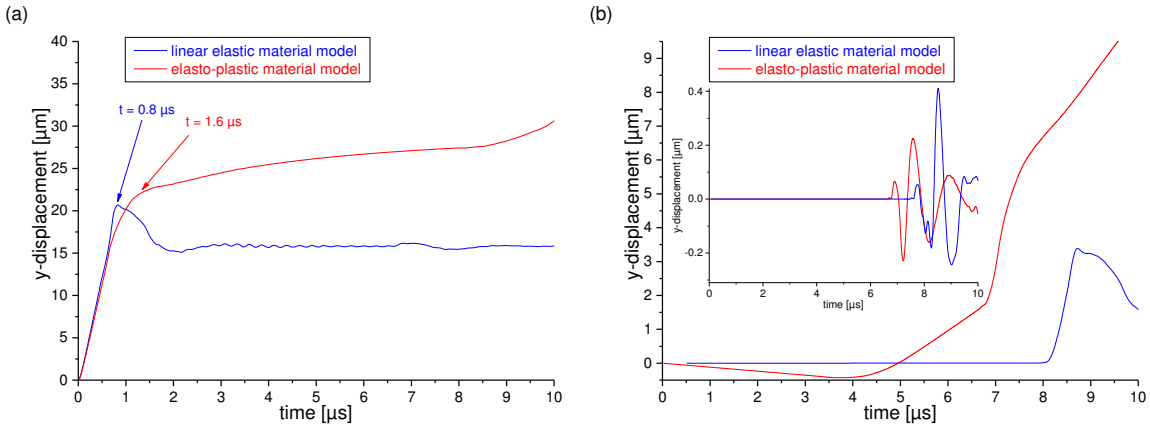

Fig. 6. Comparison of source displacement (a) and surface displacement at (x,y) = (0,50) mm (b) for linear elastic and elasto-plastic material models.

4. Summary and Conclusion

Using the maximum y-displacement values of the cases with linear-elastic material properties presented in figure 4 and figure 5 the relation between the maximum internal (source) displacement and the external (surface) displacement can be evaluated. A summary of these calculations and for some intermediate values is given in figure 7. While for the variation of external force a direct linear relationship is observed, this is not the case for the variation of crack length. For the latter the maximum surface displacement seems to follow a $x^{3/2}$ relationship on the maximum source displacement. This is not in agreement with the usual expectations of analytical theories (e.g. Green and Zerna [17]). However, this relationship is a consequence of the description of active crack growth, which is not taken into account for the respective analytical theories [8,17].

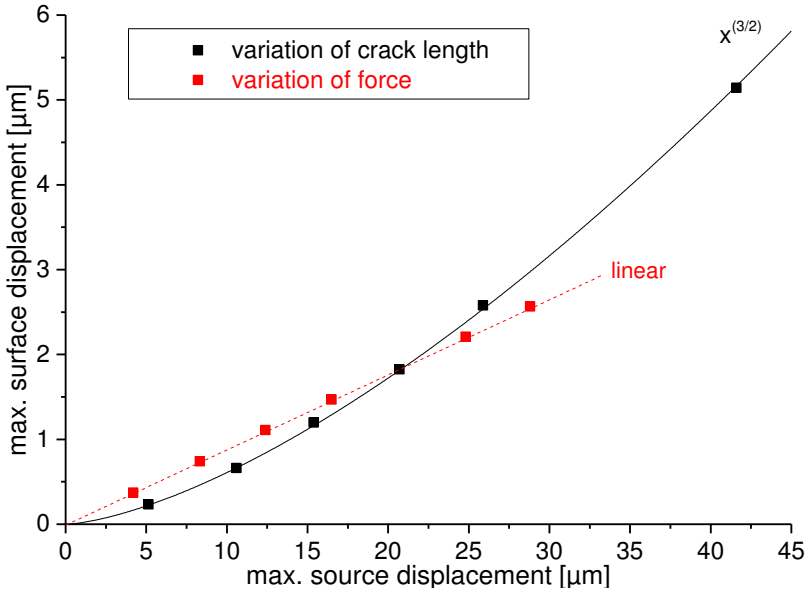

Fig. 7. Relation between the maximum source displacement and the maximum AE amplitude for an observation point in 50 mm distance.

The modeling of plastic deformation during crack propagation reveals further contributions of the displacement field not covered by present theories. The large deviation between the linear elastic model and the elasto-plastic model for the aluminum alloy demonstrates the importance of this contribution.

With the present model an improved description of the acoustic emission release due to the process of crack formation is possible. The insight gained by such modeling work aids in the interpretation of the physical processes and allows assessing the impact of the material properties on the acoustic emission signals. Careful revision has to be done concerning the direct estimation of source rise-times and source strengths based on static calculations derived from fracture mechanics.

Acknowledgments

I would like to thank Marvin Hamstad for the fruitful discussions on acoustic emission sources and Siegfried Horn for the continuous support to carry out independent research in the field of acoustic emission.

References

[1] K. Aki, P. G. Richards. Quantitative seismology, theory and methods. University Science Books, Sausalito, 1980.

[2] M. Giordano, A. Calabro, C. Esposito, A. D'Amore, L. Nicolais. An acoustic-emission characterization of the failure modes in polymer-composite materials. Composites Science and Technology, **58**, 1923-1928, 1998.

[3] M. Ohtsu, K. Ono. The generalized theory and source representation of acoustic emission. Journal of Acoustic Emission, **5**, 124-133, 1986.

[4] M. Lysak. Development of the theory of acoustic emission by propagating cracks in terms of fracture mechanics. Engineering Fracture Mechanics, **55**:3, 443-452, 1996.

[5] M. Hamstad, A. O'Gallagher, J. Gary. Modeling of Buried Acoustic Emission Monopole and Dipole Sources With a Finite Element Technique, Journal of Acoustic Emission, **17**:3-4, 97-110, 1999.

[6] M. Hamstad. On Lamb Modes as a Function of Acoustic Emission Source Rise Time, Journal of Acoustic Emission, **27**, 114-136, 2009.

[7] M. Ohtsu, K. Ono. A generalized theory of acoustic emission and Green's function in a half space. Journal of Acoustic Emission, **3**, 27-40, 1984.

[8] C. Scruby. Quantitative Acoustic Emission Techniques, Nondestructive Testing, **8**, 141-210, 1985.

[9] P. Wilcox, C. Lee, J. Scholey, M. Friswell, M. Wisnom, B. Drinkwater. Progress Towards a Forward Model of the Complete Acoustic Emission Process, Advanced Materials Research, **13-14**, 69-76, 2006.

[10] W. Prosser, M. Hamstad, J. Gary, A. O'Gallagher. Comparison of Finite Element and Plate Theory Methods for Modeling Acoustic Emission Waveforms, Journal of Nondestructive Evaluation, **18**:3, 83-90, 1999.

[11] P. Hora, O. Cervena. Acoustic emission source modeling, Applied and Computational Mechanics, 4, 25-**36**, 2010.

[12] M. Sause and S. Horn. Simulation of acoustic emission in planar carbon fiber reinforced plastic specimens, Journal of Nondestructive Evaluation, **29**:2, 123-142, 2010.

[13] M. Sause, M. Hamstad, S Horn. Finite element modeling of lamb wave propagation in anisotropic hybrid materials, Composites Part B: Engineering, **53**, 249-257, 2013.

[14] G. McLaskey, S. Glaser. Acoustic Emission Sensor Calibration for Absolute Source Measurements, Journal of Nondestructive Evaluation, **31**:2, 157-168, 2012.

[15] O. Cervena, P. Hora. Analysis of the conical piezoelectric acoustic emission transducer, Applied and Computational Mechanics, **2**, 13-24, 2008.

[16] M. Sause, M. Hamstad, S. Horn. Finite element modeling of conical acoustic emission sensors and corresponding experiments, Sensors and Actuators A: Physical, **184**, 64-71, 2012.

[17] A. Green, W. Zerna. Theoretical Elasticity, Oxford University Press, London and New York, 1954.